



TECHNICAL ARTICLE

Investigation of the Crevice Corrosion Behavior of 316L Stainless Steel in Sulfate-Reducing Bacteria-Inoculated Artificial Seawater Using the Wire Beam Electrode

Zhan Zhang, Cong Wu, Zhaopeng Wang, Jiuyang Xia, Bowei Zhang, and Junsheng Wu

Submitted: 3 December 2021 / Revised: 5 April 2022 / Accepted: 5 May 2022 / Published online: 31 May 2022

Keywords 316L, artificial seawater, crevice corrosion, sulfate-reducing bacteria (SRB)

1. Introduction

316L stainless steel (316LSS) is known for its excellent corrosion resistance and has been widely used in marine engineering (Ref 1). But 316LSS tends to suffer from local corrosion in seawater environment, especially crevice corrosion, which often causes unexpected harm. Compared with the open environment, the local micro-environment within the crevice is more unpredictable due to complex influencing factors, such as the geometric size of the crevice, pH value, temperature, and oxygen concentration (Ref 2-5). However, previous research has hardly paid attention to the influence of microbial factors on crevice corrosion, which cannot be ignored in the actual seawater environment.

In recent years, microbiologically influenced corrosion has been extensively studied in the open environment. As the most widespread corrosive bacteria, sulfate-reducing bacteria (SRB) has been widely reported (Ref 6-11). The polarization resistance of 316LSS immersed in the sterile solution was considerably higher than that immersed in the SRB-inoculated solution (Ref 12). Furthermore, it had been reported that stainless steel had a significantly higher corrosion rate in the SRB-inoculated solution due to the corrosive sulfide produced by the SRB (Ref 13-15). Several corrosion mechanisms have been proposed, such as the cathodic depolarization theory, the biogenic hydrogen sulfide theory, and the biocatalytic cathodic sulfate reduction theory, greatly advancing comprehension of SRB-induced corrosion (Ref 16-20). The oxygen-free environment within the crevice may be more conducive to the survival of anaerobic bacteria such as SRB. SRB is undoubtedly the best

choice for studying the influence of microbial factors on crevice corrosion.

The wire beam electrode (WBE) technology can be used to measure the distribution and changing process of electrochemical information of the electrode surface (Ref 21). The application of WBE in localized corrosion, such as crevice corrosion and concrete localized corrosion, has made great research progress (Ref 22-29).

In this study, the potential-current distribution within the crevice was mapped by using the WBE, and the influence of the SRB's distribution on the crevice corrosion of 316LSS was discussed.

2. Experimental Methods

2.1 Bacterium and Culture Medium

The SRB strains were obtained from the China General Microbiological Culture Collection Center (CGMCC). The preparation of the seawater culture medium required the mixing of two solutions. Solution A consisted of 0.5 g K_2HPO_4 , 1.0 g NH_4Cl , 1.0 g Na_2SO_4 , 0.1 g $CaCl_2 \cdot 2H_2O$, 2.0 g $MgSO_4 \cdot 7H_2O$, 2.0 g DL-sodium lactate, 1.0 g yeast extract, 0.1 g sodium thioglycolate, and 0.1 g vitamin C into 0.5 L deionized water. Solution B was prepared by adding 24.53 g NaCl, 5.20 g $MgCl_2$, 4.09 g Na_2SO_4 , 1.16 g $CaCl_2$, 0.695 g KCl, 0.201 g $NaHCO_3$, and 0.101 g KBr into 0.5 L deionized water. The two solutions were adjusted to a pH of 7.0 ± 0.2 with $0.1 \text{ mol} \cdot L^{-1}$ NaOH and were autoclaved at 121 °C for 20 min, respectively. Finally, solutions A and B were mixed to 1 L to prepare the seawater culture medium in an anaerobic environment. The SRB was inoculated into the seawater culture medium and cultured in anaerobic bottles at 37 °C.

2.2 Materials and Crevice Former

316LSS was adopted as the experimental material. The chemical composition (wt.%) of 316LSS, determined by the spark discharge atomic emission spectrometric method, was C 0.03, Si 1.0, Mn 2.0, Cr 17.0, Mo 2.50, Ni 12.0, P 0.045, S 0.03, and Fe balanced.

The WBE consisted of 100 stainless steel wires and were regularly arranged as a 10 x 10 matrix and inserted in epoxy

Zhan Zhang and Cong Wu are equally contributed to this work.

Zhan Zhang, Cong Wu, Zhaopeng Wang, Jiuyang Xia, Bowei Zhang, and Junsheng Wu, Institute for Advanced Materials and Technology, University of Science and Technology Beijing, Beijing 100083, China. Contact e-mails: bwzhang@ustb.edu.cn and wujs@ustb.edu.cn.

resin with an interval of 1mm from each other. The schematic diagram is shown in Fig. 1. The surface of the WBE was sequentially abraded by 200, 400, 800, and 1500 grit water sandpapers and was cleaned with ultrasonic waves in acetone and absolute ethanol. The crevice width was chosen to be 200 μm , which was based on the possibility of the SRB can just enter. A U-shaped PTFE gasket with a thickness of 200 μm and a square PMMA plate completely covered the WBE to form a crevice former.

In addition, 316LSS was cut into a block sample with a size of $20 \times 20 \times 3$ mm, equal to the effective working area of the WBE, combined with the same PTFE gasket and PMMA plate to form a crevice structure to observe the distribution of the SRB and corrosion morphology.

According to the different distances to the crevice mouth, the specimen surfaces were divided into three regions, namely, crevice mouth (region A), crevice inner (region B), and crevice bottom (region C).

2.3 Electrochemical Measurements

The potential and current distribution was tested by the potential–current analyzer (Corrtest Company, CST520). Electrochemical impedance spectroscopy (EIS) was conducted on a three-electrode cell in the SRB-inoculated artificial seawater using an electrochemical station (Autolab, PGSTAT302N), with the 316LSS wires samples as the working electrode, platinum foil as the counter electrode, and a saturated calomel electrode (SCE) as the reference electrode. EIS was performed by applying a voltage signal of 10 mV in the range of 100 kHz–10 mHz, and the number of points per frequency decade was 10.

2.4 Surface Analysis

The simulated samples were put into the SRB-inoculated artificial seawater to conduct immersion tests. In order to ensure that the concentration of SRB maintained a high level, half of the original SRB-inoculated solution was replaced with a new artificial seawater culture medium every 7 d.

The simulated samples were removed from the SRB-inoculated artificial seawater after the immersion tests and were cleaned in phosphate buffered saline solution to wash down the planktonic bacteria. Then, the samples were immersed in a 2.5% glutaraldehyde solution for 12 h and were then dehydrated with 50, 70, 80, 90, and 95 ethanol for 10 min and 100% ethanol for 30 min. The surface morphology was observed by scanning electron microscopy (SEM) (FEI, Quanta250).

After immersion for 30 d, the composition of the corrosion products formed in the SRB-inoculated solution was analyzed by x-ray photoelectron spectroscopy (XPS). XPS (ESCLAB

250) was conducted with an Mg-K α x-ray source at 15 kV and 150 W. The charging shifts were corrected with the C 1s peak at 284.8 eV as a reference. XPS-PEAK 4.1 software was employed to process and fit the photoelectron peaks. The spot size of the x-ray beam was 650 μm , and the pressure in the analysis chamber was maintained at $10^{-7} - 10^{-9}$ torr during each measure.

The three-dimensional morphology of the 316LSS surface was obtained by a confocal laser scanning microscopy (CLSM) (KENYENCE, VKX), and the numbers and depths of corrosion pits on the stainless steel surfaces were characterized by CLSM.

3. Results and Discussion

3.1 Distribution of the SRB within the Crevice

Figure 2 depicts the SEM images of different regions within the crevice after immersion for 30 d. In the crevice mouth, the SRB was aggregated. A small number of the SRB were distributed in the crevice inner, and almost no bacteria were distributed in the crevice bottom, implying that SRB attachment and survival were more difficult with increasing distance from the crevice mouth.

3.2 Distribution of the Current and Potential in the Crevice

Figure 3 shows the corrosion potential–current distribution of the WBE after immersion for different times in the SRB-inoculated artificial seawater. It was found that the corrosion potential and current were unevenly distributed during the immersion test and changed with time. On the 3 d, a more negative potential area and an anode current appeared in the crevice bottom, indicating that the corrosion initially occurred in the crevice bottom. According to the critical crevice solution theory (CCST), the deepest part in the crevice first reaches the critical crevice solution composition, and local corrosion occurs (Ref 30). At the same time, in the early stage of complete biofilm formation, the potential will shift positively (Ref 31). On the 10 d, the potential became negative and the anode current increased in the crevice inner, indicating that the corrosion occurred in these regions. Subsequently, the corrosion in the crevice inner was more serious, as shown in Fig. 3(c). At this stage, due to the presence of SRB in the crevice inner, the destruction of the passive film had been accelerated. When immersed for 30 d, the potential in the crevice bottom showed the most negative position again, implying that the environment in the crevice bottom became harsher, with the prolonging of the immersion time. It is worth mentioning that the corrosion current increases in the crevice

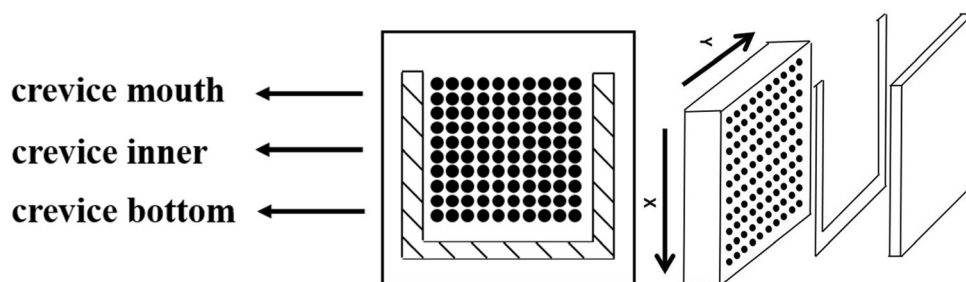


Fig. 1 Schematic diagram of the crevice former

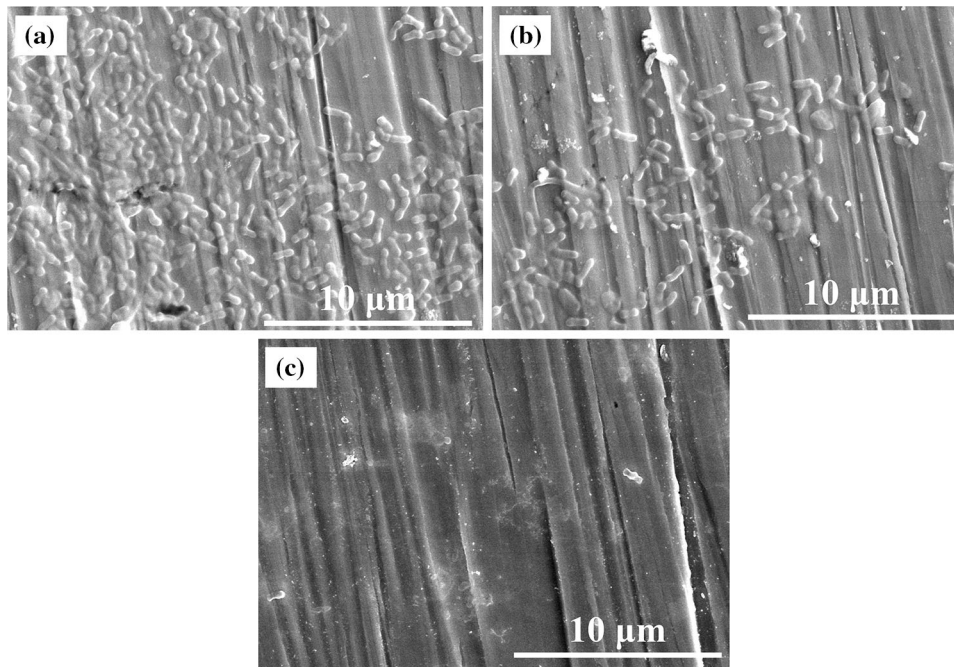


Fig. 2 SEM images of different regions in the crevice after immersion for 30 days: (a) crevice mouth; (b) crevice inner; (c) crevice bottom

mouth, which may be due to the corrosion products produced by SRB increased with the extension of time, which accelerated the corrosion in the crevice mouth.

3.3 EIS Results

EIS technology was used to further study the electrochemical behavior of 316LSS in different regions within the crevice. The WBE was immersed in the SRB-inoculated solution, and the impedance spectra were tested on the 3, 10, 20, and 30 d, respectively. Figure 4 shows the Nyquist plots of the WBE after immersion in the SRB-inoculated solution for different times. It was seen that the measured impedance plots were featured differently, depending on the region and the testing time. The larger the radius of the Nyquist semicircle, the better the corrosion resistance of the material. On the 3 d, the Nyquist diagram in the crevice bottom shows a semicircle in the high frequency region and a straight line in the low frequency region. The radius of the Nyquist semicircle in the crevice bottom was the smallest in Fig. 4(a). From days 10 to 20, the radius of the Nyquist semicircle in the crevice inner gradually decreased. During the whole corrosion process, the impedance in the crevice mouth always kept the maximum in all regions. This result was consistent with the corrosion potential–current distribution of the WEB.

To obtain impedance parameters, appropriate equivalent circuits should be used to fit the impedance data. Figure 5(a) shows the electrochemical equivalent circuits, where R_s is solution resistance, R_f and CPE_f are the resistance and capacitance of the biofilm, respectively, R_{ct} and CPE_{dl} are charge transfer resistance and double layer capacitance, respectively. The impedance of CPE_{dl} can be calculated by the Eq 1 (Ref 32):

$$Z_{CPE}(w) = Y^{-1}(jw)^{-n} \quad (\text{Eq 1})$$

where Y is the parameter similar to capacitance and n is the dispersion coefficient related to the surface inhomogeneity.

As shown in Table 1, the impedance of the passive film was similar for the three conditions (mouth, inner, and bottom) and decreased from 3 to 10 d, remained constant, and decreased again for 30 d. According to the critical crevice solution theory (CCST), the pH of the solution in the crevice will drop over time. When a certain critical value was reached, the passive film was broken. From 3 to 20 days, the pH of the solution was not low enough to break the passive film. Therefore, the impedance of the passive film remained constant. When the pH value dropped to the critical value, the impedance of the passive film decreased again. The charge transfer resistance was higher for the steel at the mouth all the time owing to the protective effect of the complete biofilm. After 3 and 10 d, the charge transfer resistance of the steel at the inner section was higher than at the bottom. After 20 d of immersion, the charge transfer resistance of steel was the same at the inner part and at the bottom, which was the result of the combined effect of microbial factors and crevice factors.

Generally, the resistance R_p , i.e., the sum of R_f and R_{ct} , can be used to evaluate the corrosion resistance of a material in corrosive environments. The R_p is inversely proportional to the corrosion rate. Figure 5(b) shows the time dependence of the fitted R_p values for the 316LSS in the SRB-inoculated solution. On the 3 d, the R_p values of the crevice bottom were the smallest, implying that the corrosion initially occurred in the crevice bottom. It was seen that the R_p of 316LSS reduced gradually with time. When WBE was immersed for 30 d, the R_p values in the crevice inner and crevice bottom were similar and significantly less than that in the crevice mouth, indicating that the corrosion mainly occurred in the crevice inner and bottom.

3.4 XPS Analysis

The spectra of Fe, Cr, and O were fitted by XPS-PEAK according to the Cui (Ref 13) and the information given in the NIST XPS database.

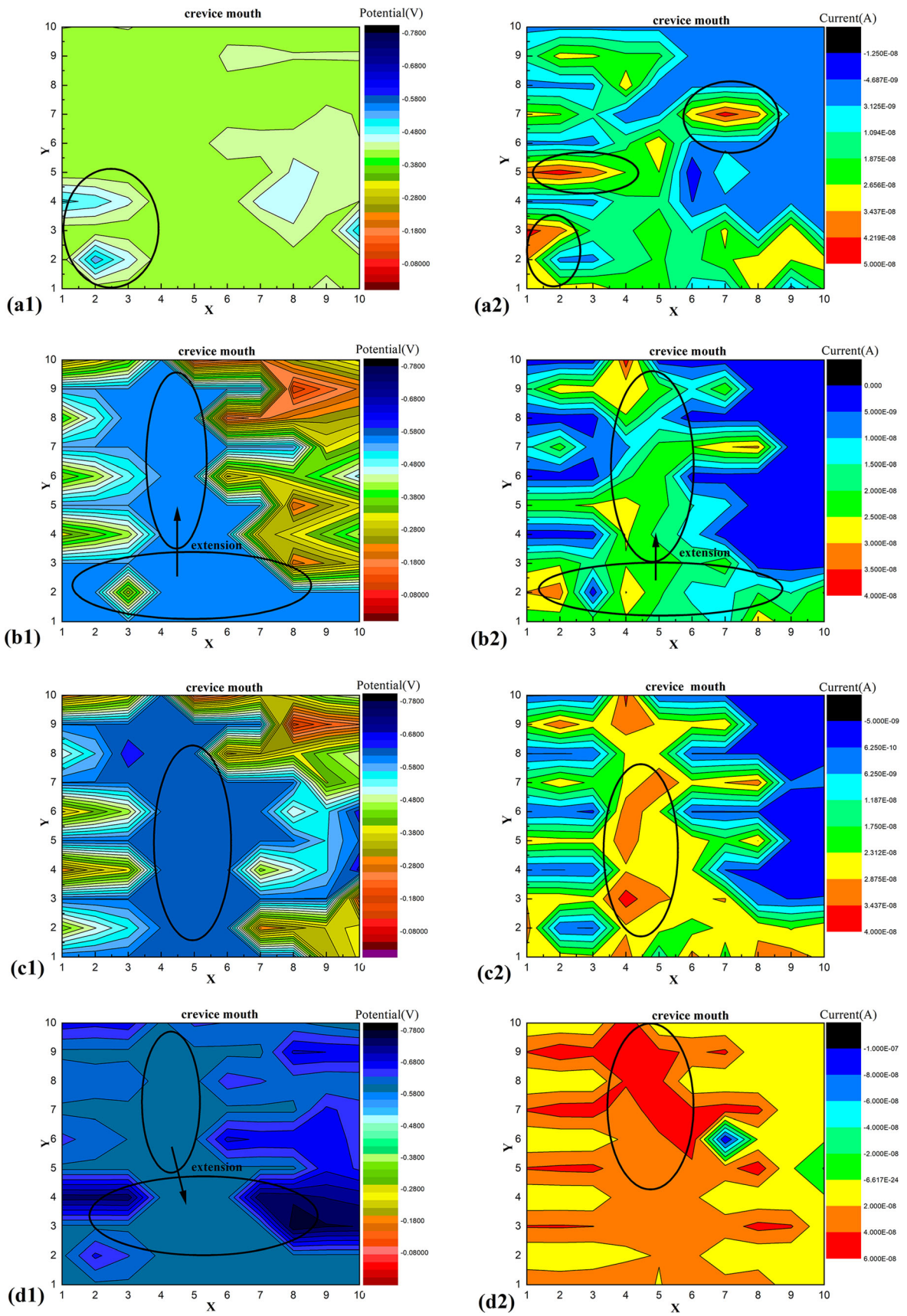


Fig. 3 The corrosion potential–current distribution of the WBE after immersion for different times: (a)3 d; (b)10 d; (c)20 d; (d)30 d

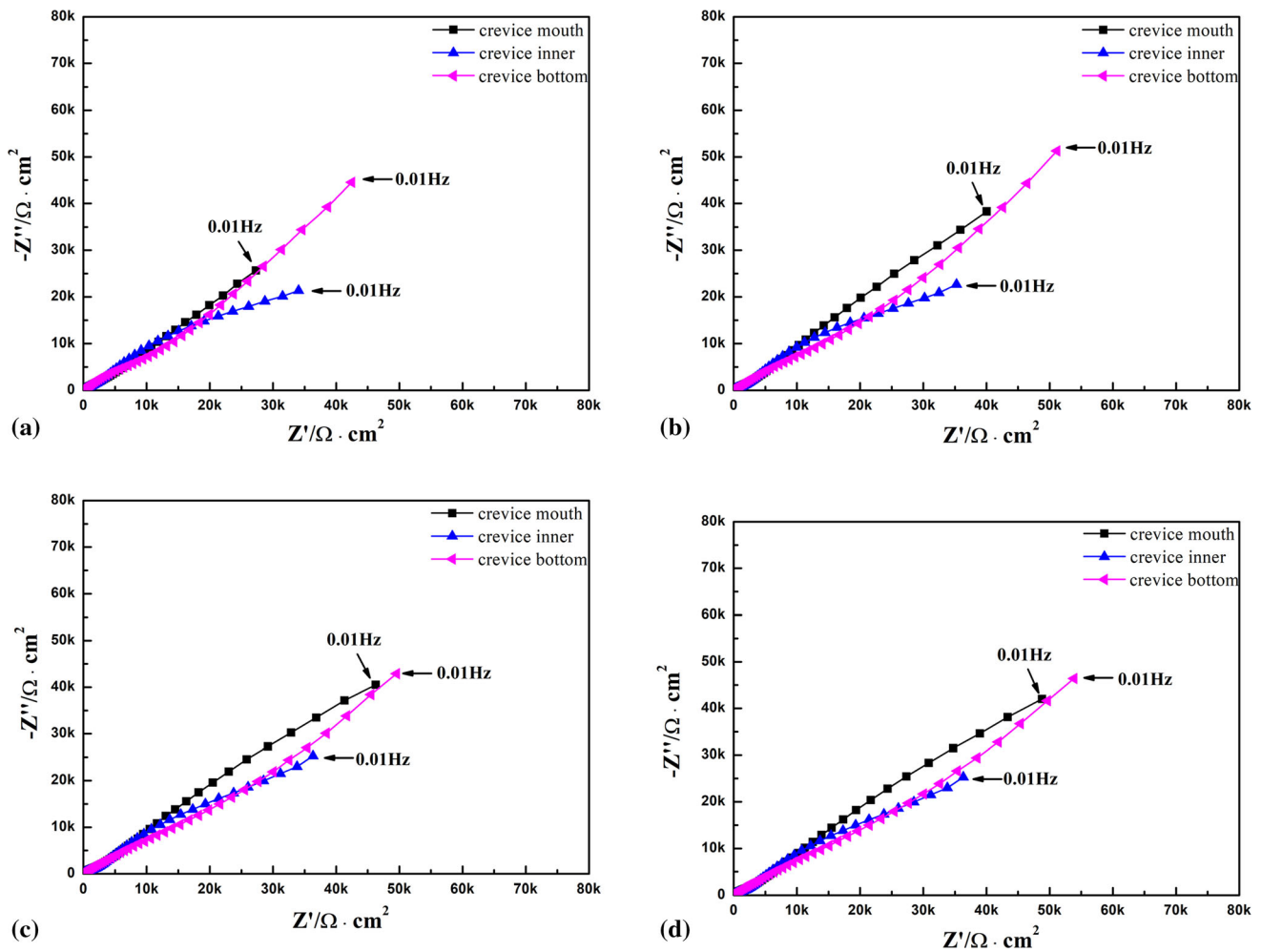


Fig. 4 Nyquist diagrams of the WBE after immersion for different times: (a) 3 d; (b) 10 d; (c) 20 d; (d) 30 d

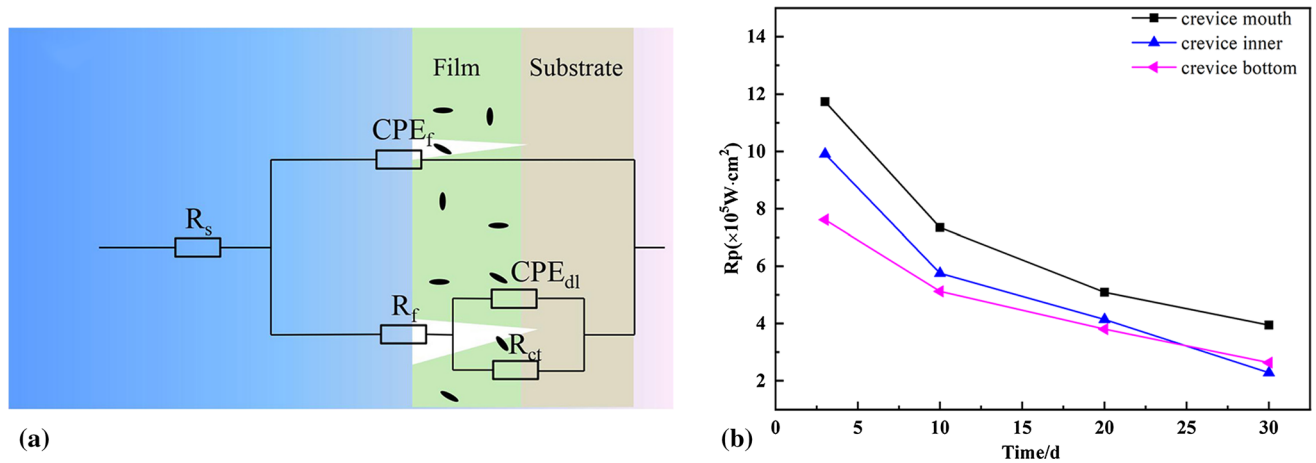


Fig. 5 (a) The electrical equivalent circuit (EEC) and (b) R_p values of the WBE immersed in the SRB-inoculated solution

Figure 6 shows the XPS spectrum of Fe 2p, Cr 2p, and O 1s of the corrosion products formed in different regions after immersing for 30 d. In Fig. 6(a1), the Fe 2p spectrum of the crevice mouth comprised $\text{Fe}(\text{OH})_3$ (712.9 eV), Fe_2O_3 (711 eV), FeO (709.5 eV), Fe_3O_4 (708.6 eV), FeS_2 (707.9 eV), and Fe^0 (706.8 eV). The content percentages obtained by calculation were 10.4, 14.2, 15.4, 25.1, 18.5, and 16.4%, respectively

(Table 2). In Fig. 6(a2), the Fe 2p spectrum of the crevice inner consisted of peak components with BEs at 712.7, 710.9, 709.4, 708.1, 707.2, and 706.5, which were attributed to $\text{Fe}(\text{OH})_3$, Fe_2O_3 , FeO, Fe_3O_4 , FeS_2 , and Fe^0 . The content percentages were 9.9, 15.2, 13.1, 21, 21.7, and 19.1%, respectively. In Fig. 6(a3), the Fe 2p spectrum of the crevice bottom comprised Fe^{2+} sat 2p (714.3 eV), $\text{Fe}(\text{OH})_3$ (712.8 eV), Fe_2O_3 (710.9 eV),

Table 1. EIS parameters of the WBE after immersion for different immersion times

Immersion time	Region	$R_s, \Omega \text{ cm}^2$	$CPE_{R_s}, \Omega^{-1} \text{ cm}^2 \text{ S}^n$	n	$R_f, \Omega \text{ cm}^2$	$CPE_{R_f}, \Omega^{-1} \text{ cm}^2 \text{ S}^n$	$R_{ct}, \Omega \text{ cm}^2$
3 d	Crevice mouth	419.2	1.09×10^{-4}	0.88	3.48×10^5	1.05×10^{-4}	8.26×10^5
	Crevice inner	520.1	3.15×10^{-4}	0.79	3.45×10^5	7.95×10^{-4}	6.46×10^5
	Crevice bottom	638.8	1.60×10^{-4}	0.84	3.39×10^5	9.21×10^{-5}	4.23×10^5
10 d	Crevice mouth	492.6	1.48×10^{-4}	0.82	2.58×10^5	9.64×10^{-4}	4.77×10^5
	Crevice inner	522.9	2.41×10^{-4}	0.84	2.58×10^5	8.63×10^{-4}	3.17×10^5
	Crevice bottom	772.3	9.92×10^{-5}	0.82	2.57×10^5	2.67×10^{-4}	2.55×10^5
20 d	Crevice mouth	495.9	1.21×10^{-4}	0.90	2.65×10^5	9.03×10^{-4}	2.44×10^5
	Crevice inner	569.0	1.82×10^{-4}	0.78	2.52×10^5	8.51×10^{-4}	1.62×10^5
	Crevice bottom	774.4	7.65×10^{-4}	0.86	2.57×10^5	7.96×10^{-4}	1.23×10^5
30 d	Crevice mouth	491.8	1.09×10^{-4}	0.77	1.73×10^5	8.69×10^{-4}	2.21×10^5
	Crevice inner	559.9	1.66×10^{-4}	0.83	1.46×10^5	8.26×10^{-4}	1.17×10^5
	Crevice bottom	761.1	6.87×10^{-4}	0.82	1.11×10^5	7.80×10^{-4}	1.17×10^5

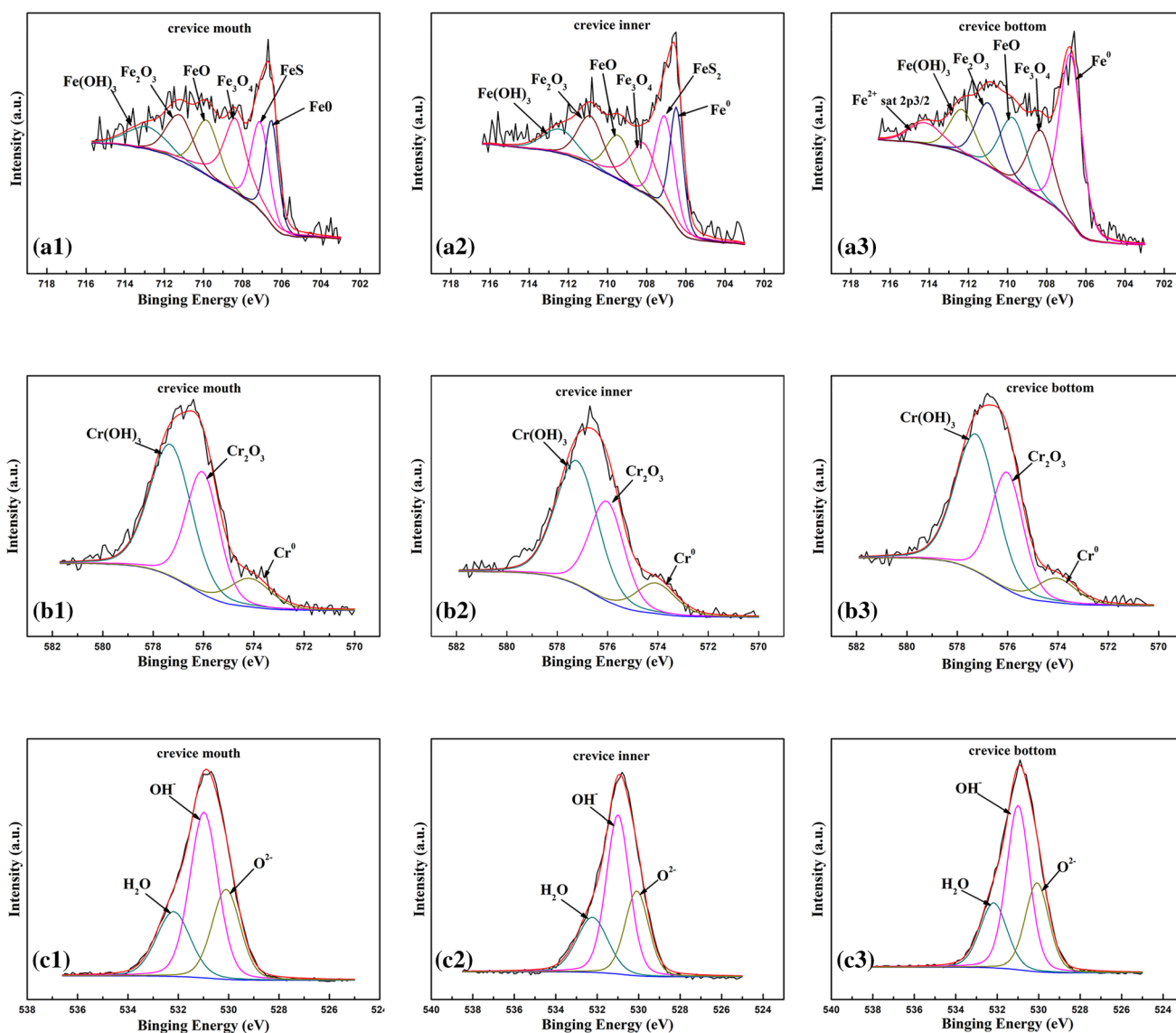


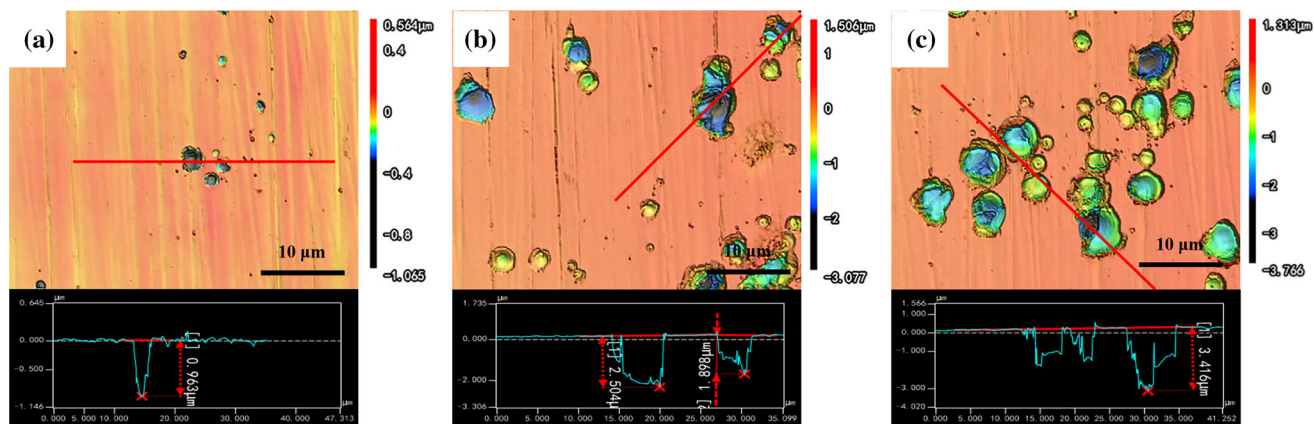
Fig. 6 XPS spectrum of Fe 2p_{3/2} (a), Cr 2p_{3/2} (b), and O 1s (c) of the corrosion products formed in different regions after immersion for 30 d

FeO (709.4 eV), Fe₃O₄ (708 eV), and Fe⁰ (706.9 eV). The content percentages were 6.7, 10.4, 15.1, 16.3, 15.9, and 35.5%. FeS₂ only existed in the crevice mouth and inner,

indicating that the SRB had adhered to in these regions and produced H₂S through the metabolism, which corresponded to the result in Fig. 2.

Table 2. The relative content (%) of Fe 2p in the passive film fitted by the XPS results

Position	Fe ²⁺	Fe(OH) ₃	Fe ₂ O ₃	FeO	Fe ₃ O ₄	FeS ₂	Fe ⁰
crevice mouth	...	10.4	14.2	15.4	25.1	18.5	16.4
crevice inner	...	9.9	15.2	13.1	21	21.7	19.1
crevice bottom	6.7	10.4	15.1	16.3	15.9	...	35.5

**Fig. 7** CLSM images and pit depth of 316L in different regions in the crevice after immersion for 30 days: (a) crevice mouth; (b) crevice inner; (c) crevice bottom

In Fig. 6(b), the Cr 2p spectrum of the 316LSS consisted of peak components with BEs at 577.7, 576.2 and 574 eV, which were attributed to Cr(OH)₃, Cr₂O₃, and Cr⁰. The content percentage of the crevice mouth were 51.4, 37.4, and 11.2%, respectively. The content percentage of the crevice inner were 52.8, 34.9, and 12.2%, respectively. In addition, the content percentage of the crevice bottom were 54.3, 36.5, and 9.2, respectively. It could be seen that there was no obvious difference in the existence and content of the Cr element in different regions.

Figure 6(c) shows the results of the O 1s spectrum of the 316LSS. The O element mainly existed in three forms in the passivation film, namely H₂O (532.5 eV), OH⁻ (531 eV), and O²⁻ (530.1 eV). The percentage content of each component in different regions was roughly the same.

3.5 Corrosion Morphology

The CLSM images and pit depths of 316LSS in the crevice after immersion for 30 d are shown in Fig. 7. In the crevice mouth, the number and size of pits on the surface were small, and the largest pit depth was only 0.963 μm. Comparatively, the number and size of pits both increased in the crevice inner. In the crevice bottom, pits were densest, and the largest pit depth was up to 3.416 μm. Therefore, according to the above results, the samples suffered obvious corrosion in the crevice inner and bottom, and corrosion in the crevice bottom was more serious.

According to CCST, the corrosion occurred preferentially in the crevice bottom because the innermost solution changed greatly and firstly reached the critical state (Ref 30). With the addition of microbial factors, a complete biofilm was formed in the crevice mouth and an incomplete biofilm was formed in the crevice inner. The reason for the lack of biofilm formation in the crevice bottom may be that the composition of the solution was not suitable for microorganisms' survival or the existence

of the crevice hindered the entry of microorganisms. Biofilms provided a protective effect in the early stages of corrosion (Ref 31). Therefore, the most serious corrosion priority occurred in the crevice bottom. With the extension of time, the production of FeS₂ under the biofilm and the change in the composition of the passive film caused the corrosion resistance of 316LSS to decrease. Galvanic effect under incomplete biofilm made it corrode faster than under complete biofilm (Ref 33). Therefore, corrosion is equally serious in the crevice inner and bottom under the synergistic effect of the microbial factors and crevice factors. The schematic diagram of the crevice corrosion in the SRB-inoculated artificial seawater is shown in Fig. 8.

4. Conclusion

The corrosion behavior of 316L stainless steel in the SRB-inoculated artificial seawater was investigated. The main conclusions are summarized as follows.

The distribution of the SRB within the crevice was uneven. The SRB was aggregated in the crevice mouth and became a complete biofilm. With increasing distance from the crevice mouth, SRB's attachment and survival were more difficult.

In the SRB-inoculated artificial seawater, corrosion preferentially occurred in the crevice bottom. And due to the existence of the SRB, corrosion began to extend to the regions near the crevice mouth. Subsequently, corrosion moved to the crevice bottom again.

The corrosion products near the crevice mouth contained FeS₂, indicating that the protective performance of the passive film was reduced. Due to the synergistic effect of the microbial factors and crevice factors, corrosion is equally serious in the crevice inner and bottom.

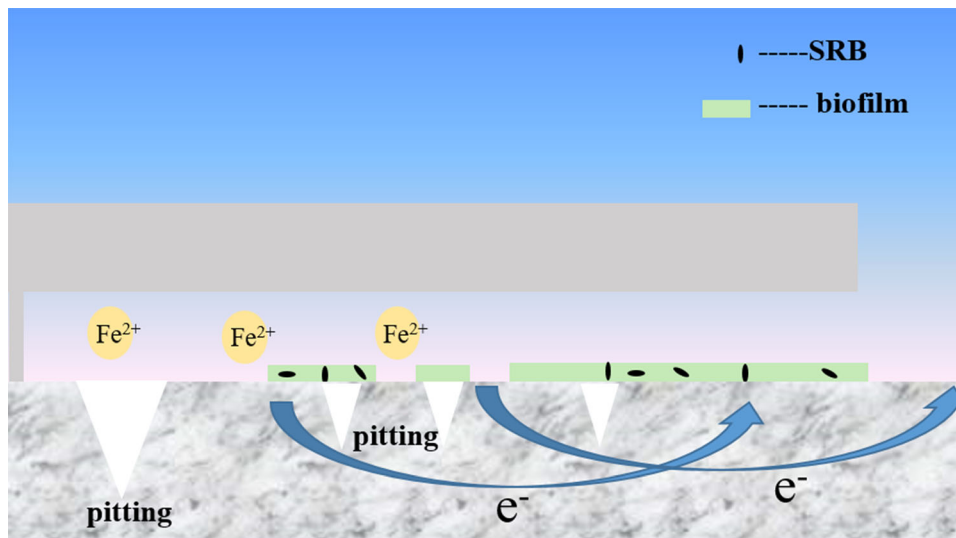


Fig. 8 Schematic diagram of the crevice corrosion in the SRB-inoculated artificial seawater

Acknowledgments

This work was supported by the National Natural Science Foundation of China (Grant No.51771027, 51901018), the Fundamental Research Funds for the Central Universities (Grant No. FRF-AT-20-07), the National Science and Technology Resources Investigation Program of China (Grant No. 2019FY101400), and China Postdoctoral Science Foundation (Grant No. 2019M660456).

Availability of Data and Material

Data and material for this manuscript will be available upon request.

Conflict of interest

The authors declare no competing financial interest.

References

- B. Zheng, K. Li, H. Liu, and T. Gu, Effects of Magnetic Fields on Microbiologically Influenced Corrosion of 304 Stainless Steel, *Ind. Eng. Chem. Res.*, 2014, **53**(1), p 48–54
- Z. Zhang, W. Rong, J. Wu, T. Zhang, Y. Wang, K. Huang, B. Zhang, and Y. He, Direct Preparation of Nanostructured Ni Coatings on Aluminium Alloy 6061 by Cathode Plasma Electrolytic Deposition, *Surf. Coatings Technol.*, 2019, **370**(4), p 130–135
- P.T. Jakobsen and E. Maahn, Temperature and Potential Dependence of Crevice Corrosion of AISI 316 Stainless Steel, *Corros. Sci.*, 2001, **43**(9), p 1693–1709
- D. Sridharan, C. Karthikeyan, S. Maruthamuthu, S. Manoharan, and N. Palaniswamy, Impact of Mixed Inhibitor on Electrochemical Behavior of Inland Water Biofilm Formed on 316L Stainless Steel, *Ind. Eng. Chem. Res.*, 2013, **52**(46), p 16175–16181
- D. Han, Y.M. Jiang, C. Shi, B. Deng, and J. Li, Effect of Temperature, Chloride Ion and PH on the Crevice Corrosion Behavior of SAF 2205 Duplex Stainless Steel in Chloride Solutions, *J. Mater. Sci.*, 2012, **47**(2), p 1018–1025
- D. Enning and J. Garrelfs, Corrosion of Iron by Sulfate-Reducing Bacteria: New Views of an Old Problem, *Appl. Environ. Microbiol.*, 2014, **80**(4), p 1226–1236
- R. Jia, D. Yang, J. Xu, D. Xu, and T. Gu, Microbiologically Influenced Corrosion of C1018 Carbon Steel by Nitrate Reducing Pseudomonas Aeruginosa Biofilm under Organic Carbon Starvation, *Corros. Sci.*, 2017, **127**(7), p 1–9
- H. Venzlaff, D. Enning, J. Srinivasan, K.J.J. Mayrhofer, A.W. Hassel, F. Widdel, and M. Stratmann, Accelerated Cathodic Reaction in Microbial Corrosion of Iron Due to Direct Electron Uptake by Sulfate-Reducing Bacteria, *Corros. Sci.*, 2013, **66**, p 88–96
- T. Wu, J. Xu, C. Sun, M. Yan, C. Yu, and W. Ke, Microbiological Corrosion of Pipeline Steel under Yield Stress in Soil Environment, *Corros. Sci.*, 2014, **88**, p 291–305
- F. Guan, X. Zhai, J. Duan, J. Zhang, K. Li, and B. Hou, Influence of Sulfate-Reducing Bacteria on the Corrosion Behavior of 5052 Aluminum Alloy, *Surf. Coatings Technol.*, 2017, **316**, p 171–179
- M. Taleb-Berrouane, F. Khan, K. Hawboldt, R. Eckert, and T.L. Skovhus, Model for Microbiologically Influenced Corrosion Potential Assessment for the Oil and Gas Industry, *Corros. Eng. Sci. Technol.*, 2018, **53**(5), p 378–392
- K. Huang, D. Peng, Z. Yao, J. Xia, B. Zhang, H. Liu, Z. Chen, F. Wu, J. Wu, and Y. Huang, Cathodic Plasma Driven Self-Assembly of HEAs Dendrites by Pure Single FCC FeCoNiMnCu Nanoparticles as High Efficient Electrocatalysts for OER, *Chem. Eng. J.*, 2021, **425**(8), p 131533–131539
- L.Y. Cui, Z.Y. Liu, D.K. Xu, P. Hu, J.M. Shao, C.W. Du, and X.G. Li, The Study of Microbiologically Influenced Corrosion of 2205 Duplex Stainless Steel Based on High-Resolution Characterization, *Corros. Sci.*, 2020, **174**(4), p 108842–108852
- S. Yuan, B. Liang, Y. Zhao, and S.O. Pehkonen, Surface Chemistry and Corrosion Behaviour of 304 Stainless Steel in Simulated Seawater Containing Inorganic Sulphide and Sulphate-Reducing Bacteria, *Corros. Sci.*, 2013, **74**, p 353–366
- X. Yang, J. Shao, Z. Liu, D. Zhang, L. Cui, C. Du, and X. Li, Stress-Assisted Microbiologically Influenced Corrosion Mechanism of 2205 Duplex Stainless Steel Caused by Sulfate-Reducing Bacteria, *Corros. Sci.*, 2020, **173**(12), p 108746–108763
- T. Gu, R. Jia, T. Unsal, and D. Xu, Toward a Better Understanding of Microbiologically Influenced Corrosion Caused by Sulfate Reducing Bacteria, *J. Mater. Sci. Technol.*, 2019, **35**(4), p 631–636
- W. Dou, J. Liu, W. Cai, D. Wang, R. Jia, S. Chen, and T. Gu, Electrochemical Investigation of Increased Carbon Steel Corrosion via Extracellular Electron Transfer by a Sulfate Reducing Bacterium under Carbon Source Starvation, *Corros. Sci.*, 2019, **150**(10), p 258–267
- H. Liu, T. Gu, G. Zhang, H. Liu, and Y.F. Cheng, Corrosion of X80 Pipeline Steel under Sulfate-Reducing Bacterium Biofilms in Simulated CO₂-Saturated Oilfield Produced Water with Carbon Source Starvation, *Corros. Sci.*, 2018, **136**(12), p 47–59
- T. Černoušek, R. Shrestha, H. Kovářová, R. Špánek, A. Ševců, K. Sihelská, J. Kokinda, J. Stouřil, and J. Steinová, Microbially Influenced Corrosion of Carbon Steel in the Presence of Anaerobic Sulphate-Reducing Bacteria, *Corros. Eng. Sci. Technol.*, 2020, **55**(2), p 127–137

20. D. Xu and T. Gu, Carbon Source Starvation Triggered More Aggressive Corrosion against Carbon Steel by the *Desulfovibrio Vulgaris* Biofilm, *Int. Biodeterior. Biodegrad.*, 2014, **91**, p 74–81
21. J. Xu, C. Sun, M. Yan, and F. Wang, Electrochemical Behavior of Steel A36 under Disbonded Coating in the Presence of Sulfate-Reducing Bacteria, *Mater. Chem. Phys.*, 2013, **142**(2–3), p 692–700
22. W. Shi, T.Z. Wang, Z.H. Dong, and X.P. Guo, Application of Wire Beam Electrode Technique to Investigate the Migrating Behavior of Corrosion Inhibitors in Mortar, *Constr. Build. Mater.*, 2017, **134**, p 167–175
23. Q. Zhong, Study of Corrosion Behaviour of Mild Steel and Copper in Thin Film Salt Solution Using the Wire Beam Electrode, *Corros. Sci.*, 2002, **44**(5), p 909–916
24. Y.J. Tan, An Experimental Comparison of Three Wire Beam Electrode Based Methods for Determining Corrosion Rates and Patterns, *Corros. Sci.*, 2005, **47**(7), p 1653–1665
25. J. Xia, K. Huang, Z. Yao, B. Zhang, S. Li, Z. Chen, F. Wu, J. Wu, and Y. Huang, Ternary Duplex FeCoNi Alloy Prepared by Cathode Plasma Electrolytic Deposition as a High-Efficient Electrocatalyst for Oxygen Evolution Reaction, *J. Alloys Compd.*, 2022, **891**, p 161934–161942
26. J. Li, Z. Liu, C. Du, and X. Li, Revealing Bioinorganic Interface in Microbiologically Influenced Corrosion with FIB-SEM/TEM, *Corros. Sci.*, 2020, **173**(4), p 108763–108770
27. W. Shi, Z.H. Dong, D.J. Kong, and X.P. Guo, Application of Wire Beam Electrode Technique to Investigate Initiation and Propagation of Rebar Corrosion, *Cem. Concr. Res.*, 2013, **48**, p 25–33
28. Y.J. Tan, S. Bailey, and B. Kinsella, Mapping Non-Uniform Corrosion Using the Wire Beam Electrode Method II Crevice Corrosion and Crevice Corrosion Exemption, *Corros. Sci.*, 2001, **43**(10), p 1919–1929
29. N.N. Aung and Y.J. Tan, Monitoring Pitting-Crevice Corrosion Using the WBE-Noise Signatures Method, *Mater. Corros.*, 2006, **57**(7), p 555–561
30. J. Xu, C. Sun, M. Yan, and F. Wang, Variations of Microenvironments with and without SRB for Steel Q 235 under a Simulated Disbonded Coating, *Ind. Eng. Chem. Res.*, 2013, **52**(36), p 12838–12845
31. J. Liao, H. Fukui, T. Urakami, and H. Morisaki, Effect of Biofilm on Ennoblement and Localized Corrosion of Stainless Steel in Fresh Dam-Water, *Corros. Sci.*, 2010, **52**(4), p 1393–1403
32. B. Wei, J. Xu, Q. Fu, Q. Qin, Y. Bai, C. Sun, C. Wang, Z. Wang, and W. Ke, Effect of Sulfate-Reducing Bacteria on Corrosion of X80 Pipeline Steel under Disbonded Coating in a Red Soil Solution, *J. Mater. Sci. Technol.*, 2021, **87**, p 1–17
33. Z. Zhang, T. Fang, J. Xia, B. Zhang, and J. Wu, Distribution of Sulfate-Reducing Bacteria in the Crevice and Its Effect on the Initial Corrosion Behavior of 2205 Stainless Steel in Artificial Seawater, *Mater. Corros.*, 2021, **9**, p 1–12

Publisher's Note Springer Nature remains neutral with regard to jurisdictional claims in published maps and institutional affiliations.